Application of the HEMLAB Algorithm to DPW-8 Cases with Anisotropic Adaptive Mesh Refinement

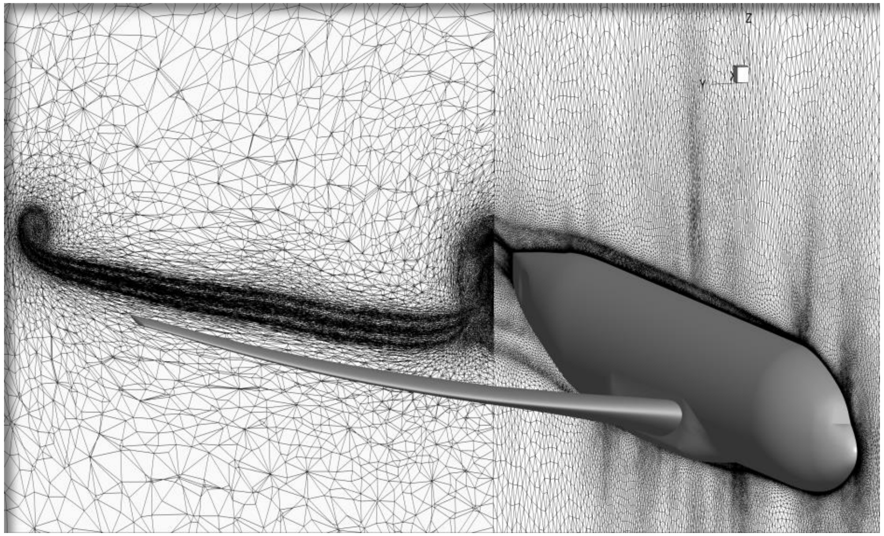

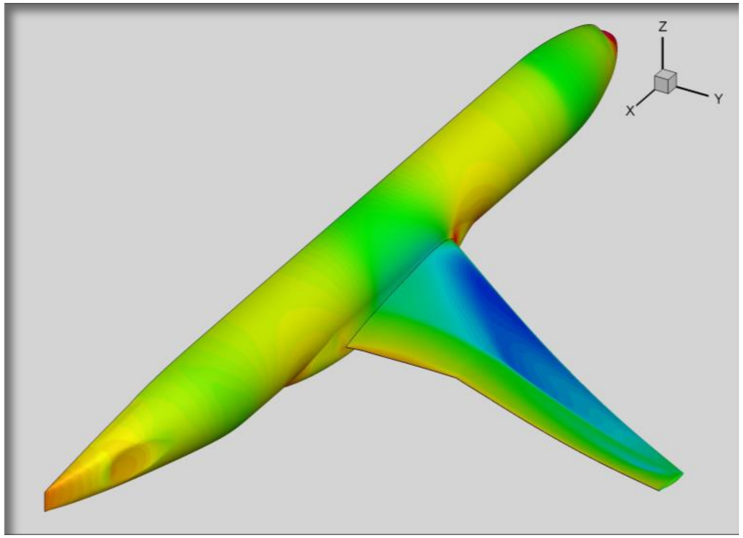

Ibrahim ASAR & Prof. Dr. Mehmet SAHİN
Faculty of Aeronautics and Astronautics,
Istanbul Technical University, 34469,
Maslak/Istanbul, TURKEY

AIAA-DPW8
6-7 June 2026, San Diego, CA

Outline

Numerical Framework:

- HEMLAB RANS Solver
- Adaptive Anisotropic Mesh Refinement (NASA Refine & INRIA pyAMG)

Test Cases:

- Case 1b – Joukowski Airfoil
- Case 1c – ONERA OAT15A Airfoil
- Case 1d – DPW-III Wing1/Wing2
- Case 2a – NASA CRM Wing-Body

Conclusions & Future Work

Numerical Method: HEMLAB Solver

Spatial Discretisation

- Vertex-centred (median-dual) finite-volume method
- Tet, prism, pyramid & hex elements – hybrid unstructured
- Edge-based data structure (cache-optimised, MPI-parallel)
- Inviscid fluxes: Roe, HLLC, AUSM$^+$-up, AUSM$^+$M, HLLC-LM
- 1st/2nd/3rd-order unweighted least-squares reconstruction
- Exact inviscid Jacobian evaluation with Tapenade library
- Limiters: Barth-Jesperson, Venkatakrishnan, Nishikawa
- Present results: 2nd-order Roe, no limiter

Nonlinear Solver

- Monolithic (fully coupled) approach
- Exact Jacobian (parallel bock matrix) assembly
- Pseudo transient continuation (PTC)
- Newton method with line-search algorithm
- GMRES + Additive Schwarz / ILU(k) preconditioner
- METIS partitioning + RCM reordering
- PETSc SNES nonlinear solver

Viscous Fluxes & Turbulence

- Green–Gauss with augmented edge-based gradients
- Avoids velocity–gradient decoupling
- Negative Spalart–Allmaras (SA-neg) model
- Exact wall-distance via Alternating Digital Tree (ADT)
- Analytical exact Jacobian

Numerical Method: Metric-Based Anisotropic Mesh Adaptation

NASA Refine (Langley)

- Riemannian metric tensor: $M(x) = R^T \Lambda R$
- Edge split/collapse/swap + node smoothing
- EGADS/EGADSlite geometry kernel (CAD-consistent)
- Fully parallel (MPI) – capable of 100M+ element meshes
- Load balancing: METIS / Zoltan
- Used for: DPW-III Wing1/Wing2 (3D)

INRIA pyAMG

- Solution-Hessian-driven metric field
- L^p-norm error estimator (p = 2 or 4)
- Anisotropic cavity-based mesh operators
- Smooth mesh transitions & high element quality
- Not parallel
- Used for: 2D airfoils + NASA CRM (3D)

Sensor Functions

- Mach number Hessian or Mach + exponential wall-distance function
- L^p-norm error estimator (p = 2 or 4)
- Identifies shocks, wakes, boundary layer regions
- Entropy sensor is also very effective for capturing rotor wakes but not used in here

Test Cases Freestream Conditions

Parameter	Case 1b Joukowski	Case 1c OAT15A	Case 1d Wing1/2	Case 2a NASA CRM
Mach number M_∞	0.15	0.73	0.76	0.85
Reynolds number Re_c	6×10^6	3×10^6	5×10^6	5×10^6
Angle of attack α	0°	1.5°	0.5°	2.5°
Temperature T [K]	322.22	271	322.22	310.93
Specific heat ratio γ	1.4	1.4	1.4	1.4
Prandtl number Pr	0.72	0.72	0.72	0.72
Turbulent Pr_t	0.9	0.9	0.9	0.9

Common to all cases: SA-neg turbulence model, Sutherland viscosity, adiabatic walls, far-field Riemann BCs

Case 1b – Joukowski Airfoil: Mesh Comparison

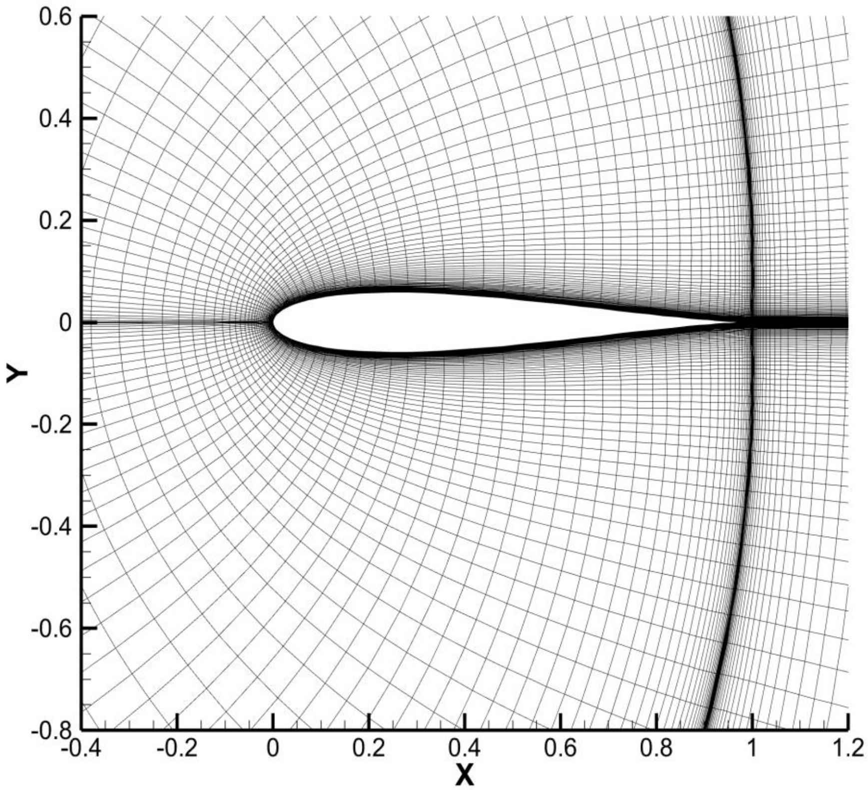

(a) Structured C-grid – 49,536 vertices

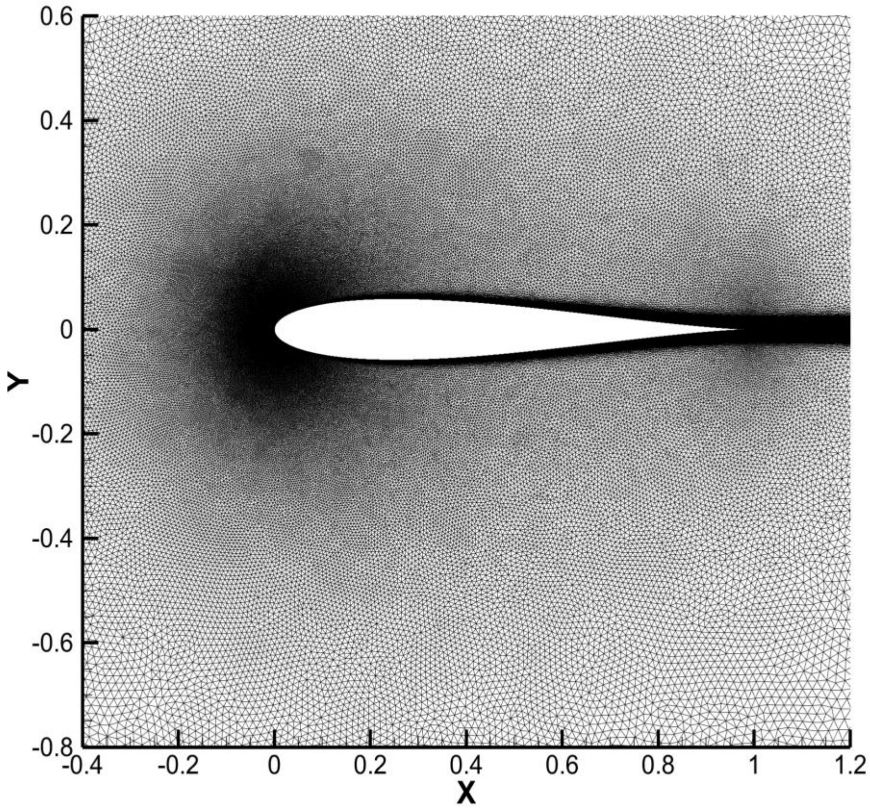

(b) pyAMG-adapted mesh – 554,113 vertices

Structured: near-orthogonal lines, smooth stretching, concentrated along chord & trailing-edge | pyAMG: fully unstructured, tight surface/wake clustering

Case 1b – Joukowski Airfoil: Flow Field Verification

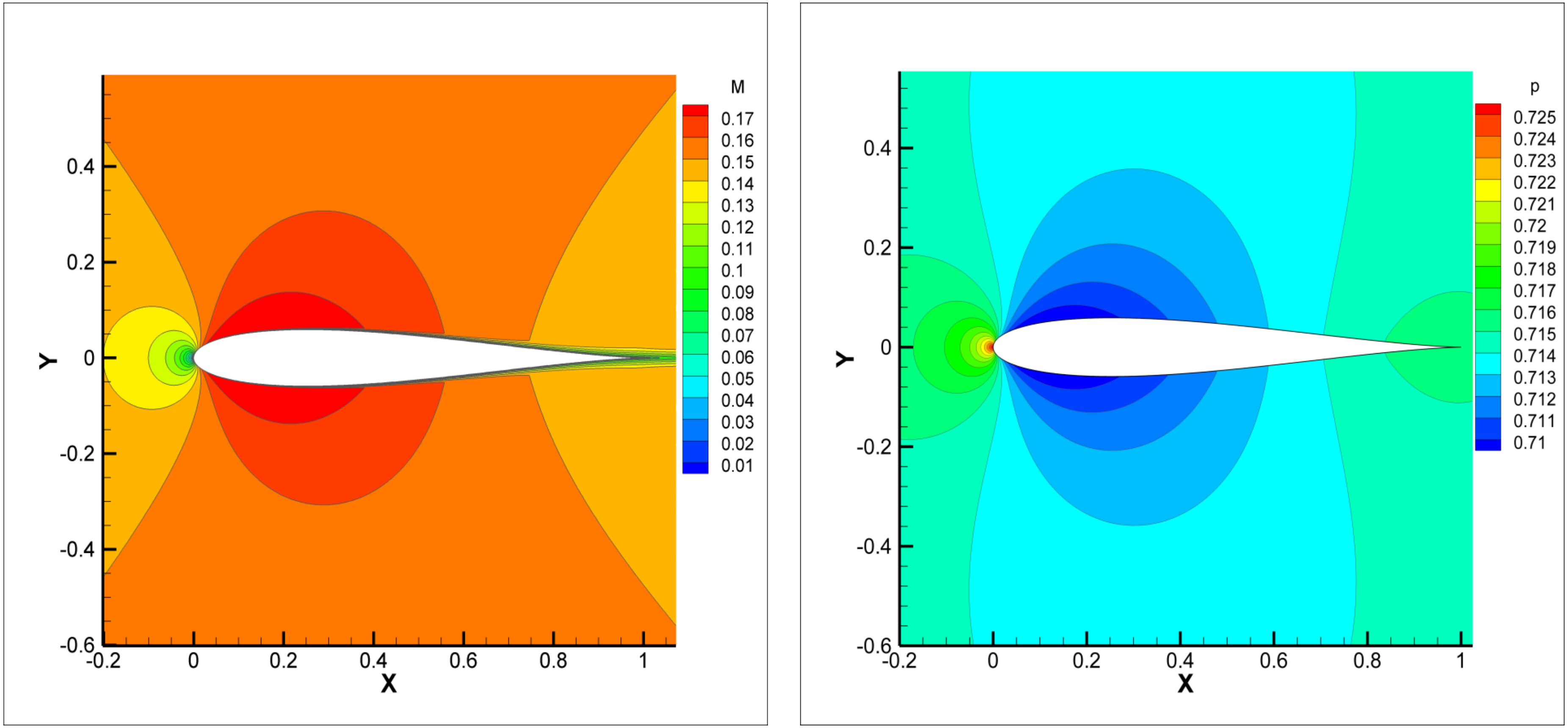

(a) Mach number *(b) Static pressure*

Contours perfectly symmetric about chord line → CL ≈ 0 confirmed · Mach rises from 0.15 to 0.17 near max thickness

Case 1b – Joukowski Airfoil: Drag Convergence (M_∞ =0.15, Re=6×10^6, α=0°)

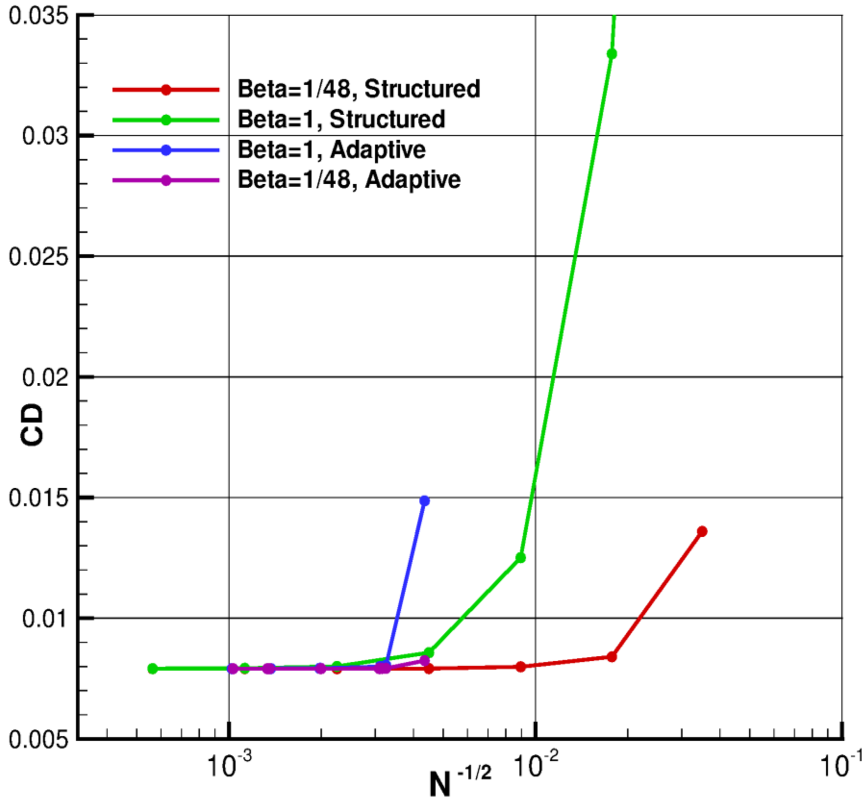

(a) Full grid-spacing range

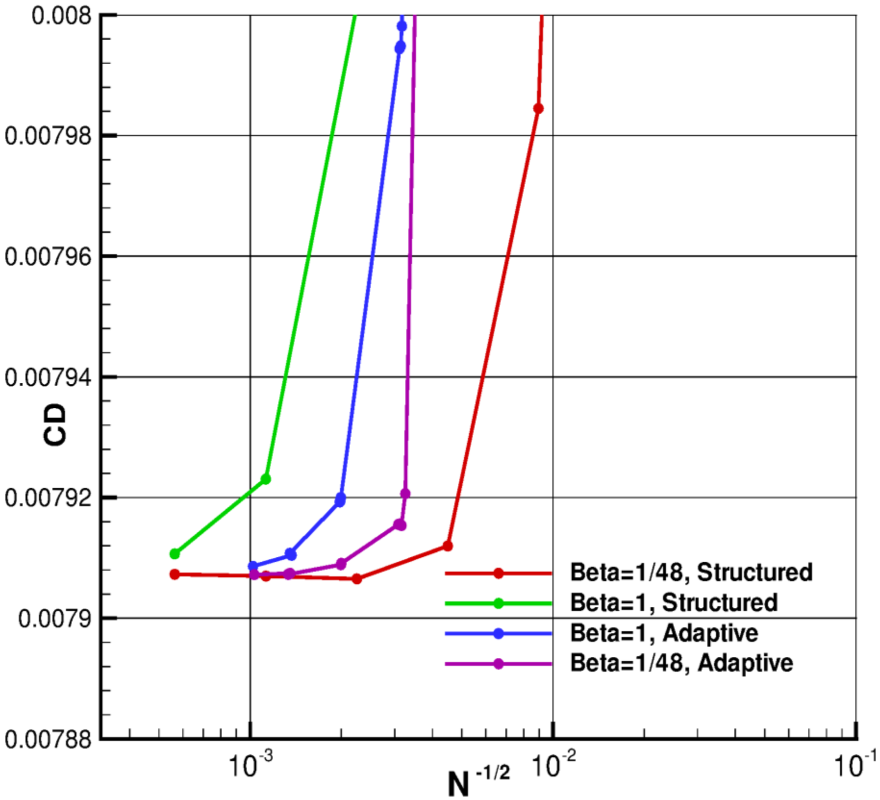

(b) Zoomed – near asymptotic value

Four datasets: structured & adaptive
- β=1/48 (almost central) and β=1 (upwind Roe)
- All converge to same asymptotic drag
- Adaptive β=1/48 reaches asymptote with ~10× fewer vertices than structured β=1

Case 1c – ONERA OAT15A: Mesh Comparison (M_∞ =0.73, Re=3×10^6, α=1.5°)

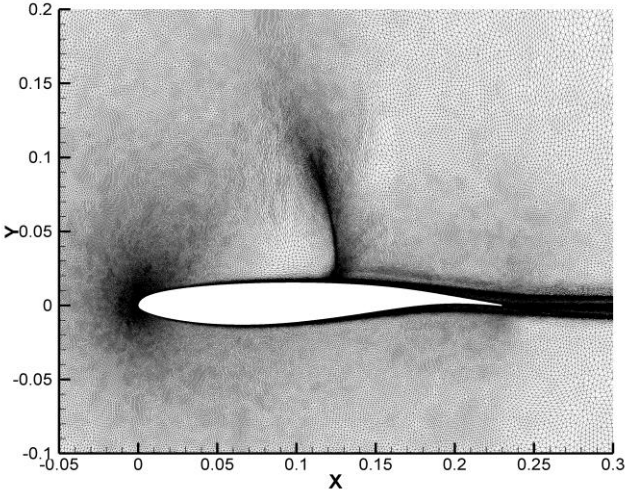

(a) pyAMG ite17 – 512,437 verts

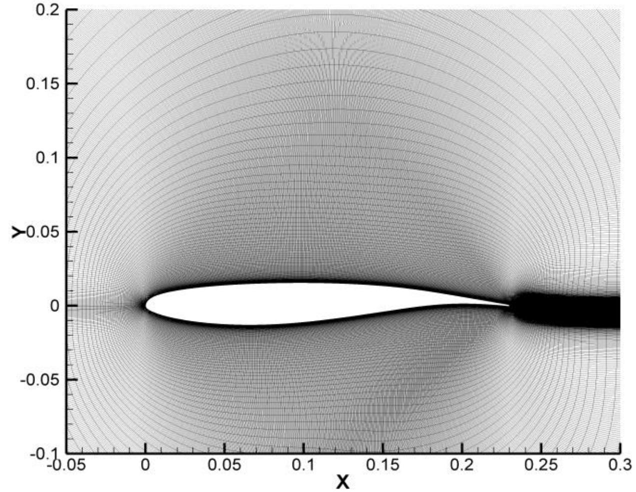

(b) Cadence L3 structured – 537,166 verts

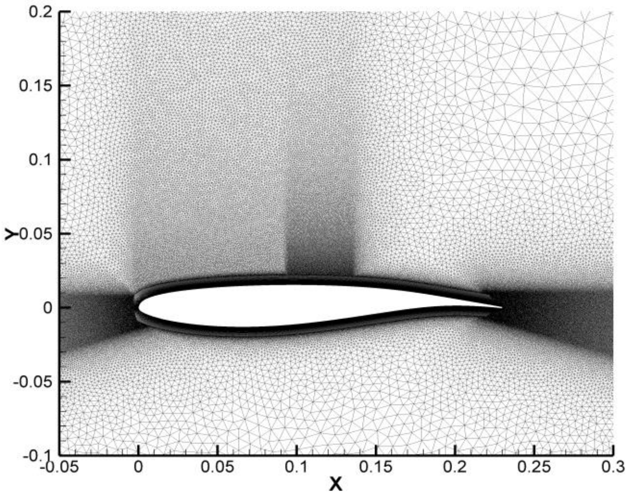

(c) Cadence L4 unstructured – 428,203 verts

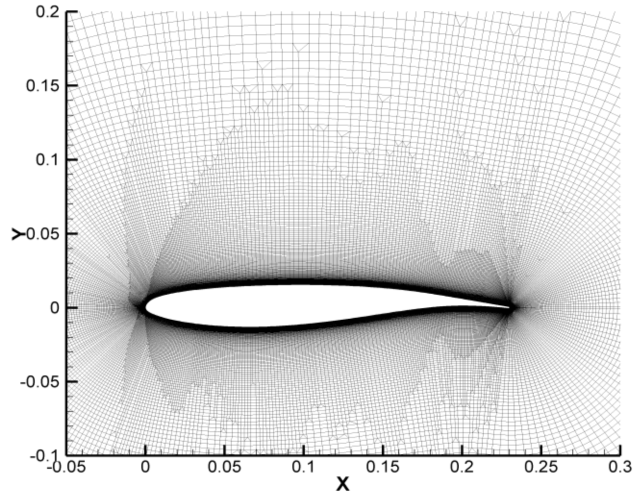

(d) Helden L6 – 411,030 verts

pyAMG mesh concentrates vertices along surface & wake; far field kept coarse · Trailing-edge resolution alone can shift predicted drag by several drag counts

Case 1c – ONERA OAT15A: Drag & Lift Convergence (M_∞=0.73, Re=3×10^6, α=1.5°)

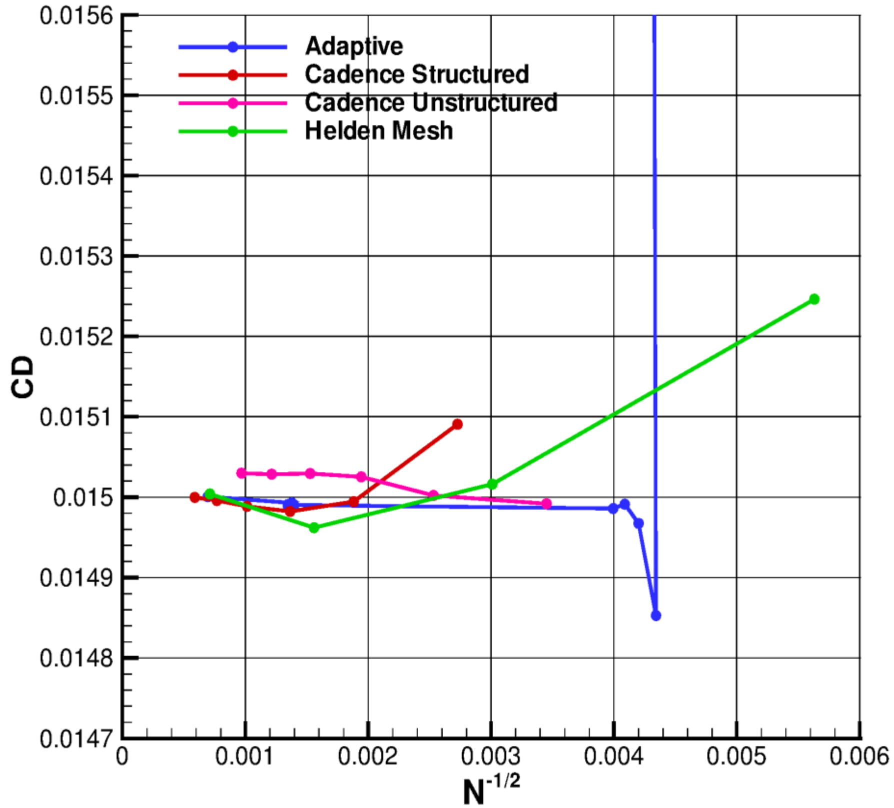

(a) Drag coefficient CD

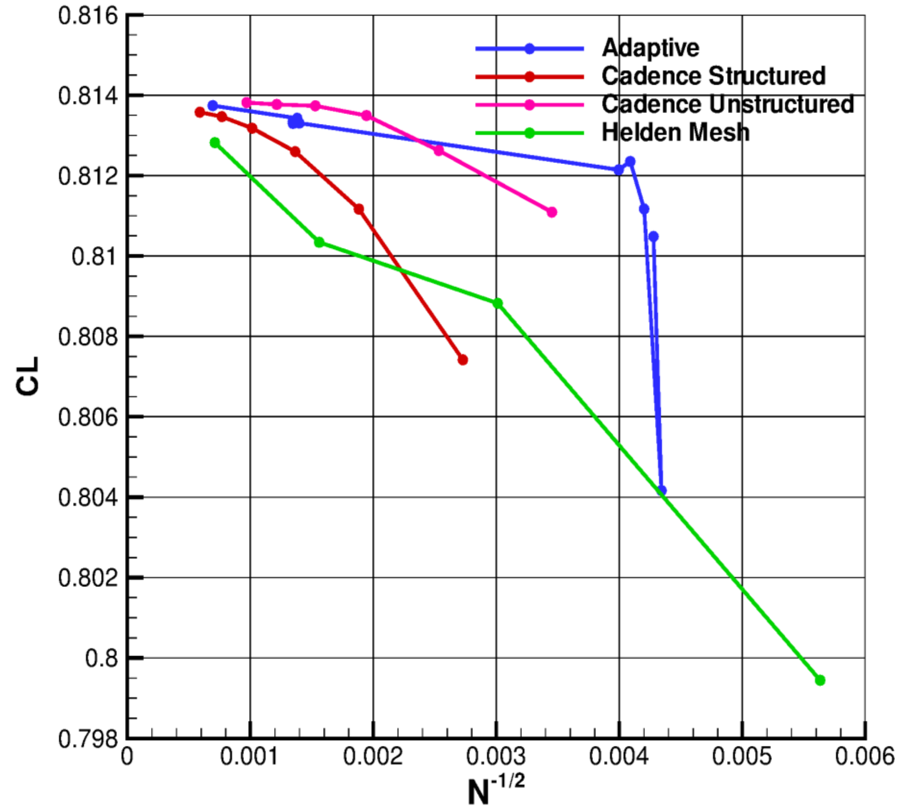

(b) Lift coefficient CL

All mesh families (structured, unstructured, pyAMG) converge toward the same asymptote · Adaptive meshes reach mesh-independent drag with significantly fewer DOFs

Case 1c – ONERA OAT15A: Trailing-Edge Close-Ups

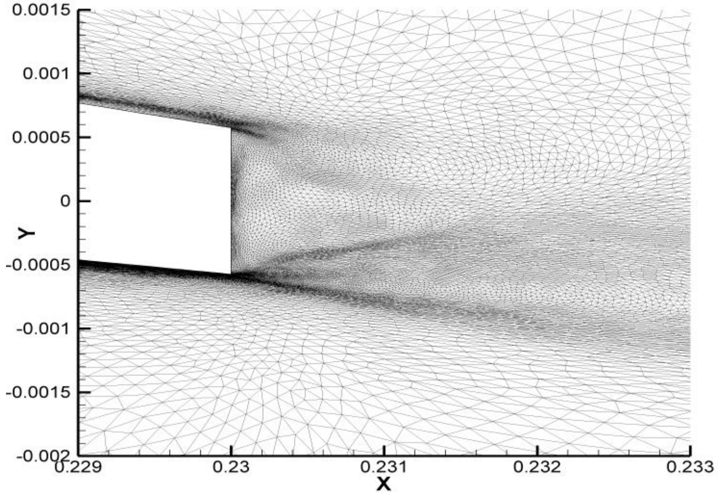

(a) pyAMG ite17

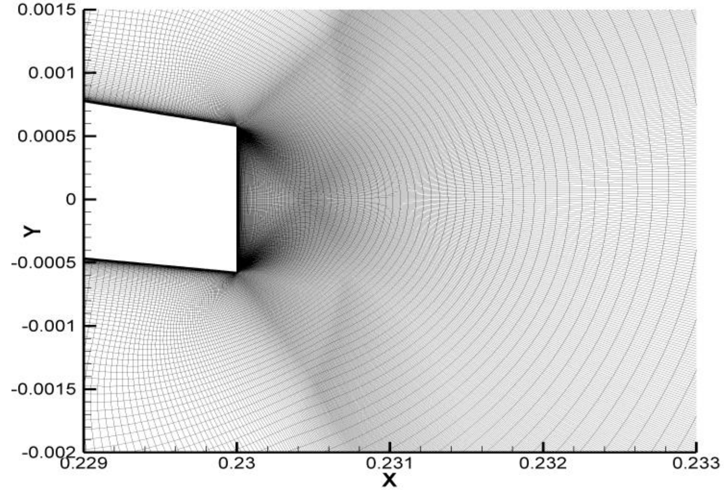

(b) Cadence L3 structured

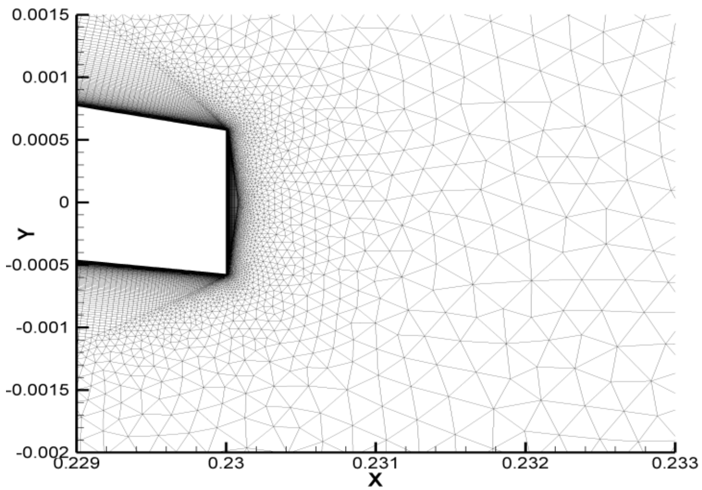

(c) Cadence L4 unstructured

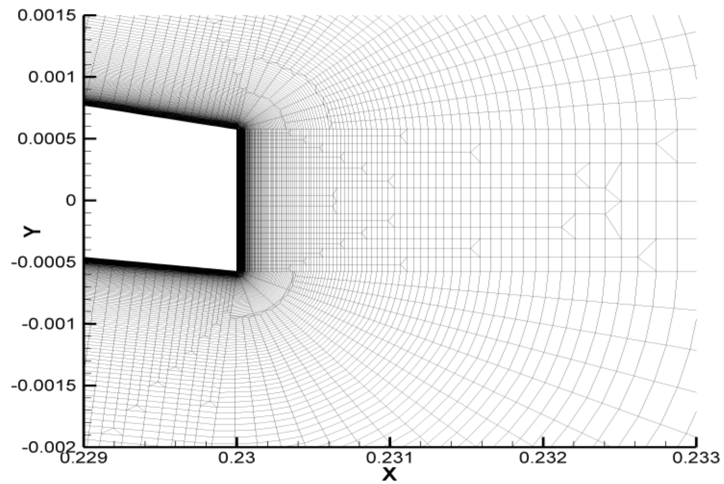

(d) Helden L6

Cadence unstructured mesh (c) has relatively larger elements at the trailing edge → slightly higher drag predictions · pyAMG achieves fine TE resolution despite comparable total vertex count

Case 1c – ONERA OAT15A: Flow Field Contours

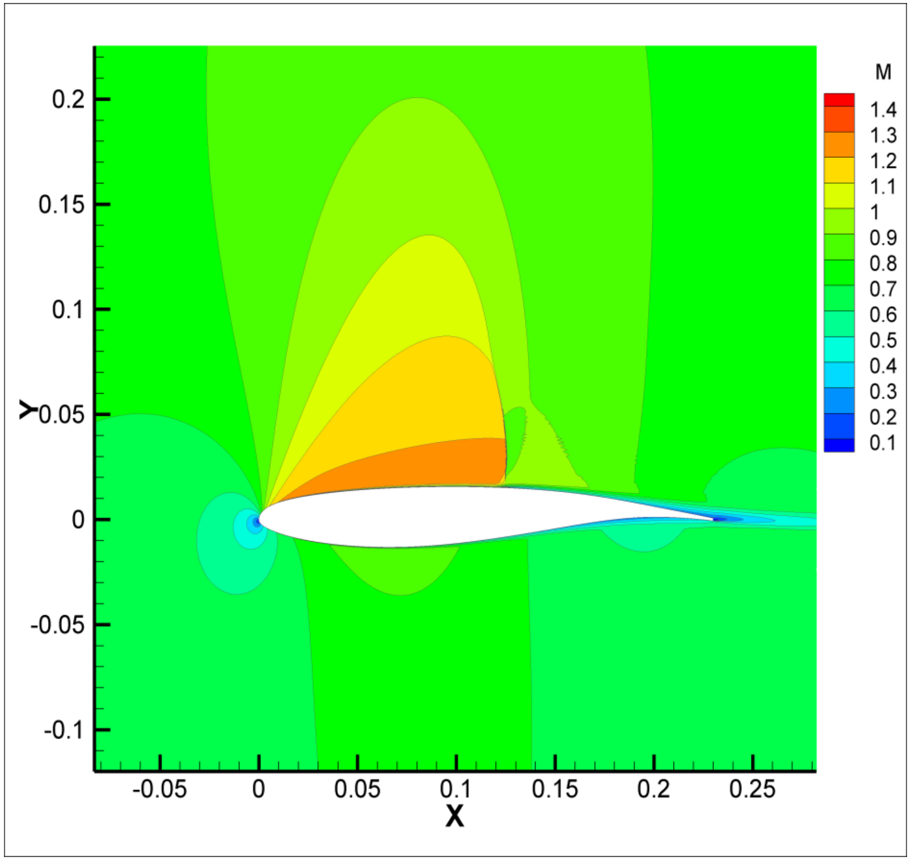

(a) Mach number

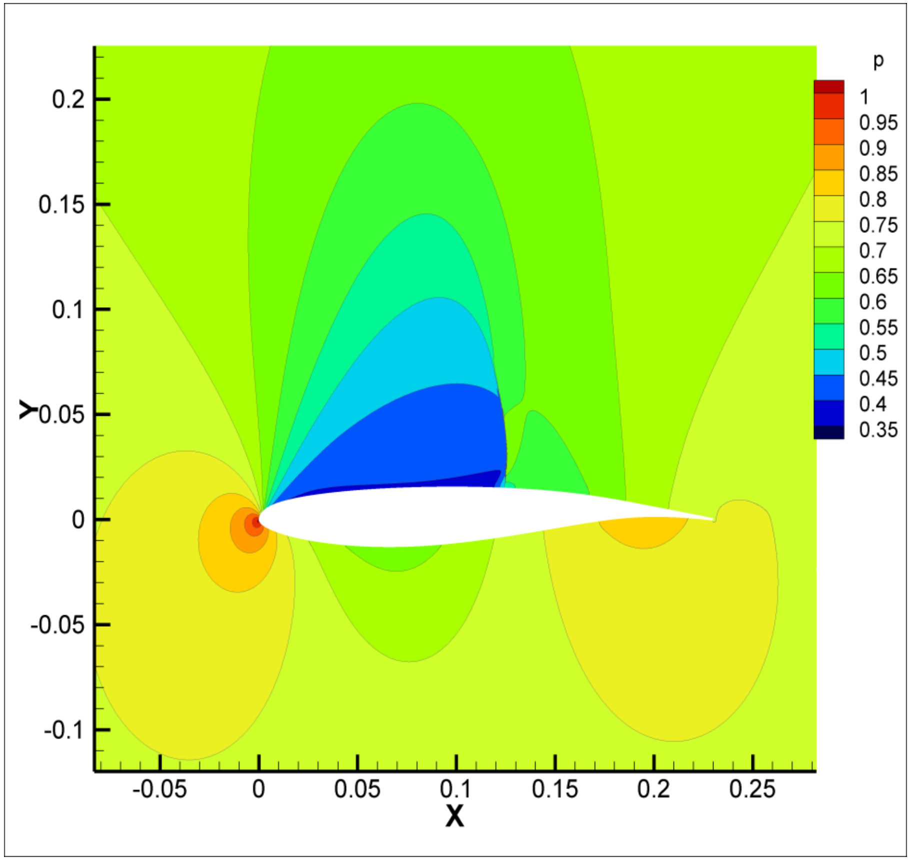

(b) Static pressure

Supersonic pocket on upper surface terminated by shock near mid-chord · Shock produces sharp pressure rise and a small separation bubble · Shock is relatively well resolved on adapted mesh

Case 1c – ONERA OAT15A: Streamlines & Shock-Induced Separation

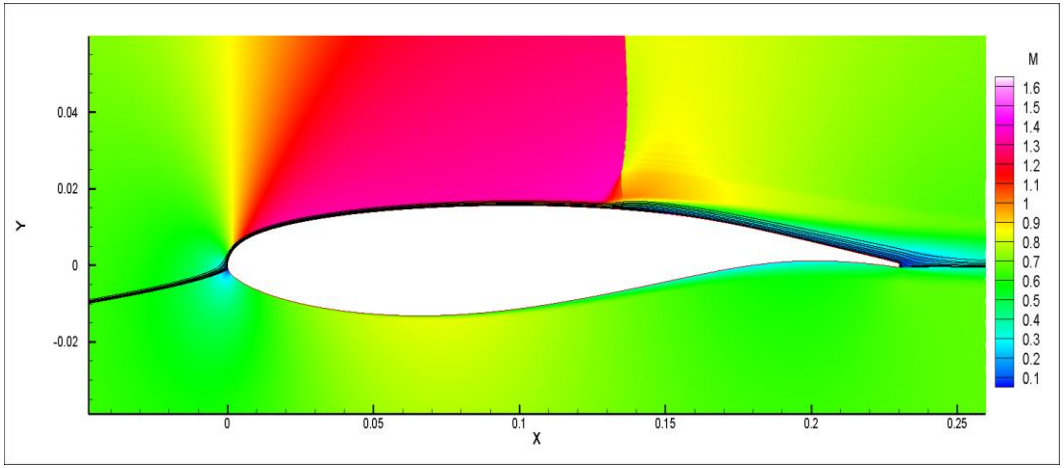

(a) Overall streamlines – α = 2.5°

α-Sweep Finding

- Increasing α: 2.5° → 3.10°
- Stronger adverse pressure gradient
- Small recirculation bubble → pronounced elongated separation region
- Shock-boundary-layer interaction intensifies

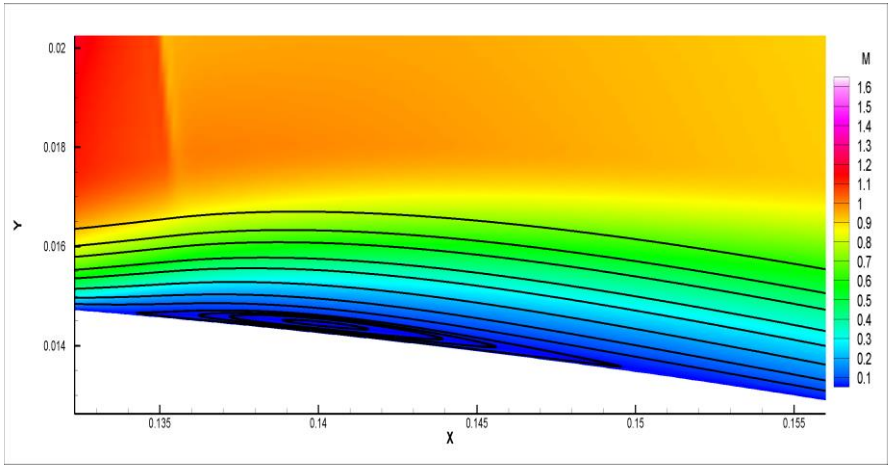

(b) Zoomed shock region – α = 2.5°

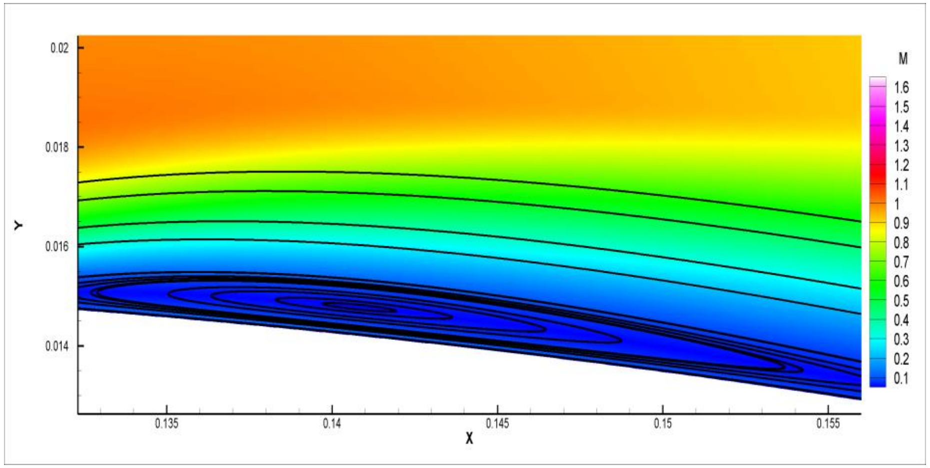

(c) Zoomed shock region – α = 3.10°

Case 1c – ONERA OAT15A: Turbulence Model Sensitivity (α=2.5°)

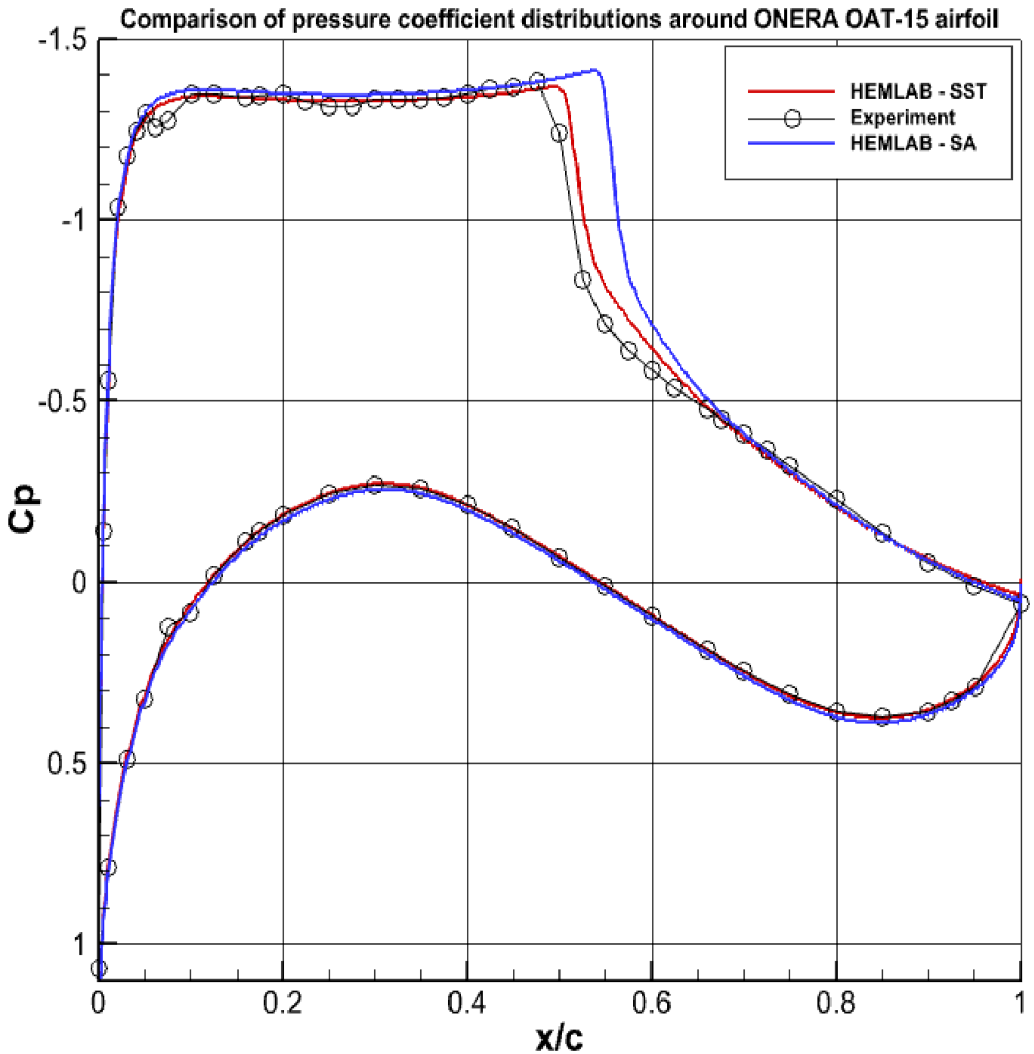

Surface Cp – SA vs. k-ω SST vs. Experiment (M=0.73, Re=3×10^6, α=2.5°)

Observations

- SA and k-ω SST yield different upper-surface shock locations
- Post-shock pressure-recovery slopes differ noticeably
- Lower surface and leading edge: essentially unaffected
- Exact ω boundary condition is used due to q=A/sqrt(ω) transformation

Important Note

- SA-neg is required for DPW-8 comparison
- Results are NOT turbulence-model-independent
- This sensitivity illustrates the importance of common modelling assumptions across participants

Case 1d – DPW-III Wing1/Wing2: Overview (M_∞ =0.76, Re=5×10^6, α=0.5°)

Configuration

- 3D transonic benchmark: two closely related wing geometries
- Goal: resolve small but persistent geometric differences in Wing1 vs. Wing2
- STEP → EGADS → TetGen coarse mesh → adaptive refinement
- Spalding wall functions for boundary-layer mesh resolution

pyAMG Gradation Study

- Two --gradation parameter values tested
- Low gradation: smoother size transitions, more conservative
- High gradation: more localised refinement around features
- Independent initial meshes from refine sequences

NASA refine Workflow

- CAD-consistent tetrahedralisation via Tetgen using EGADS/EGADSlite
- Critical for swept leading/trailing edges and wing tips
- Hessian-based metric: Mach sensor
- MPI parallel – scales to 100M+ element meshes

Key Results Preview

- Wing2 consistently produces 2.57 drag counts higher CD than Wing1
- Wing2 also produces slightly higher CL (+0.021)
- Differences persist across entire refinement sequence

Case 1d – DPW-III Wing1/Wing2: Mesh Refinement History (NASA refine)

Level	Wing 1			Wing 2		
	n_nodes	CD	CL	n_nodes	CD	CL
ini_sol	509,781	0.023740	0.46943	505,078	0.027003	0.47762
ite1	1,645,857	0.020521	0.47012	1,646,613	0.020979	0.49270
ite4	4,025,311	0.020390	0.47554	4,046,921	0.020691	0.49692
ite8	15,590,779	0.020411	0.47677	15,757,207	0.020648	0.49807
ite9	37,996,122	0.020382	0.47726	38,781,410	0.020639	0.49829
ite10	39,052,775	0.020393	0.47721	–	–	–

ite9: Wing2 CD ≈ 2.57 drag counts higher than Wing1; ΔCL ≈ +0.021 — differences small but persistent across entire refinement sequence

Case 1d – Wing1/Wing2: Force Coefficient Convergence (M_∞ =0.76, Re=5×10^6, α=0.5°)

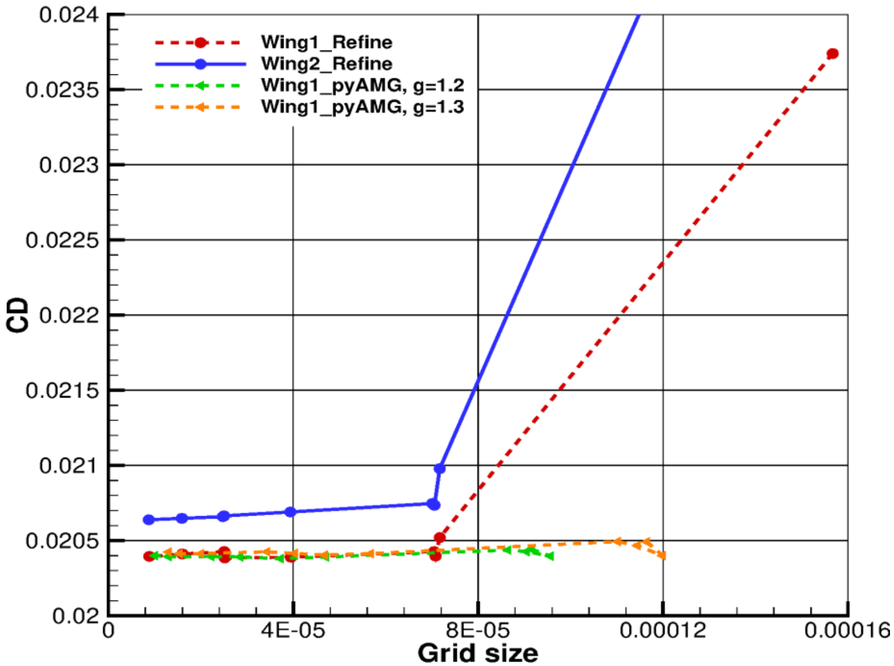

(a) Drag coefficient CD

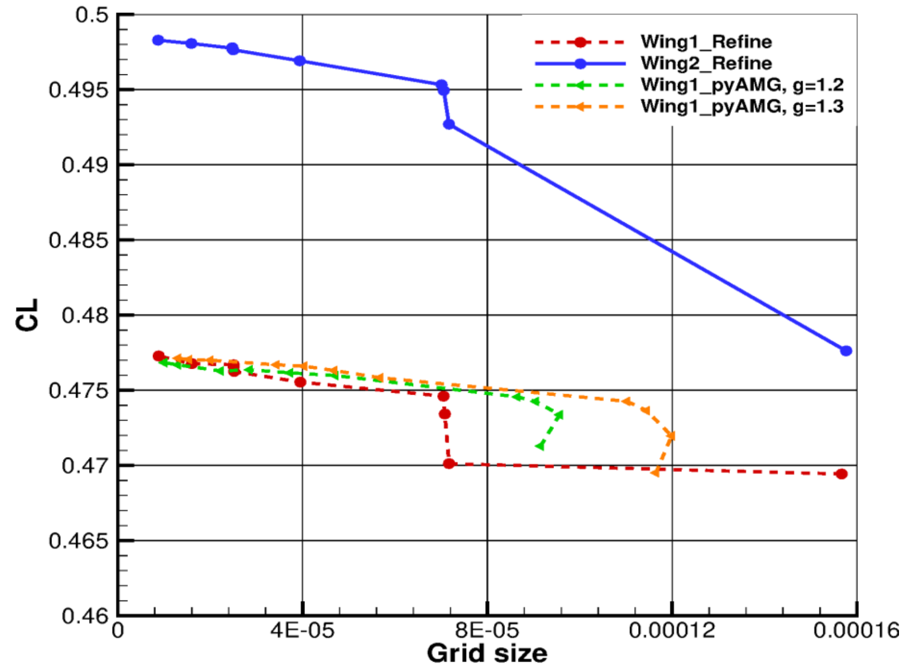

(b) Lift coefficient CL

Refine sequences show systematic convergence · pyAMG Wing1: weak sensitivity to gradation factor (less than 1 drag count)

Case 1d – DPW-III Wing1/Wing2: Residual Convergences

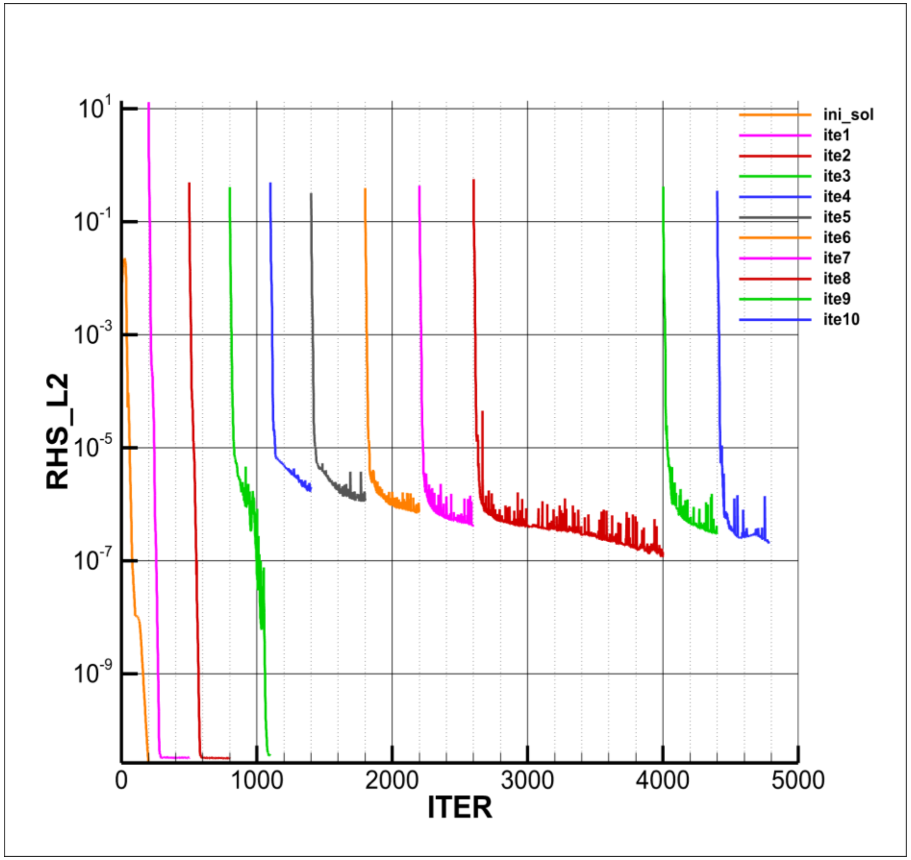

(a) Wing1 – refine adaptation runs

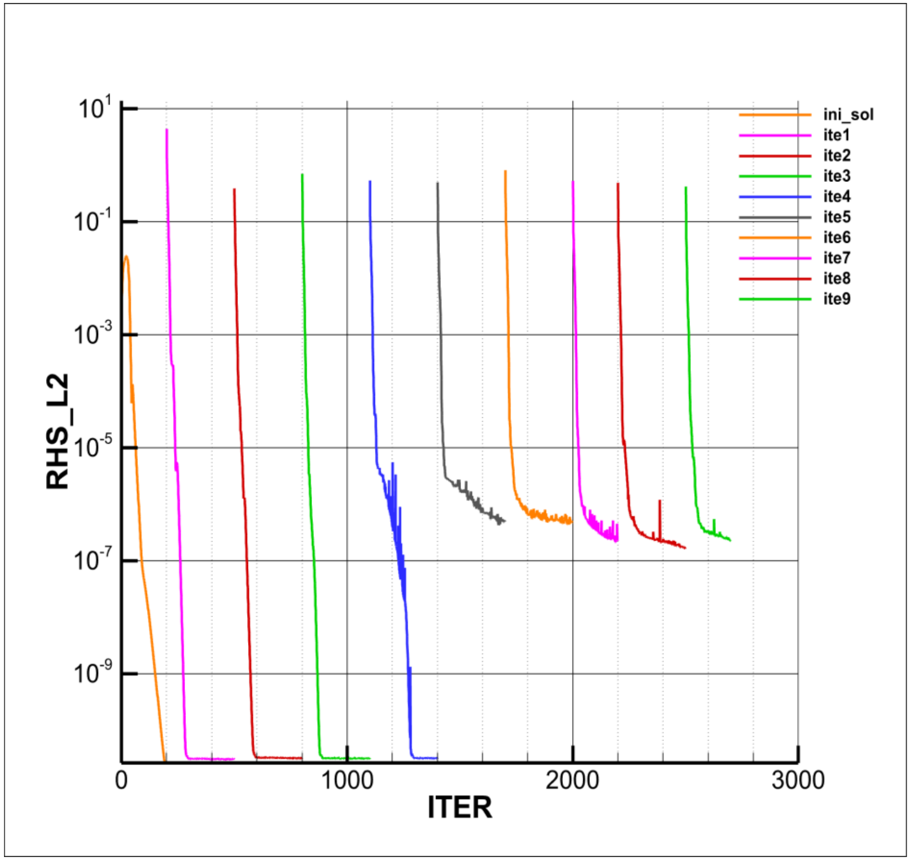

(b) Wing2 – refine adaptation runs

Several orders reduction in residual at each adaptation cycle · Residuals did not always reach machine precision – stiffness from strong anisotropic mesh refinement near shocks

Case 1d – Wing1: Adapted Volume Meshes (M_∞ =0.76, Re=5×10^6, α=0.5°)

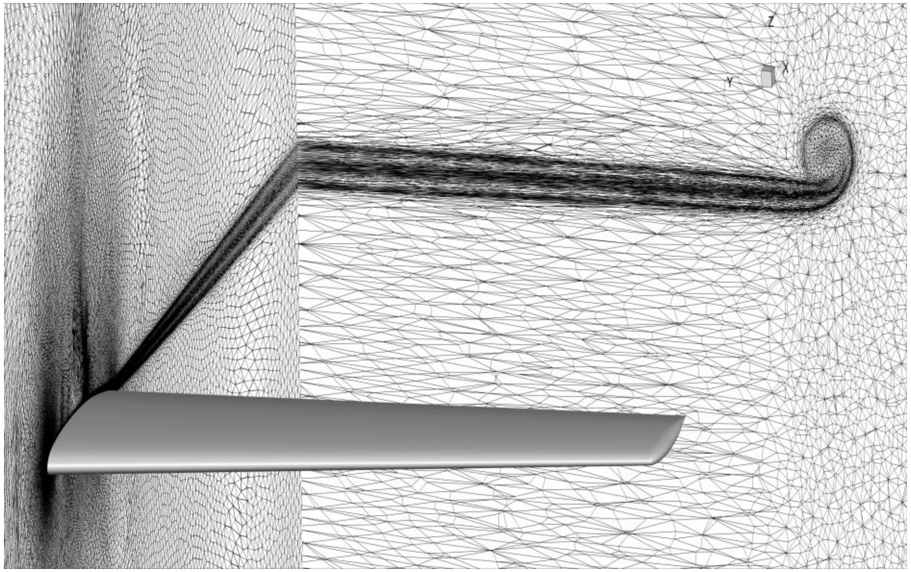

(a) refine ite8 – ~15.6 million vertices

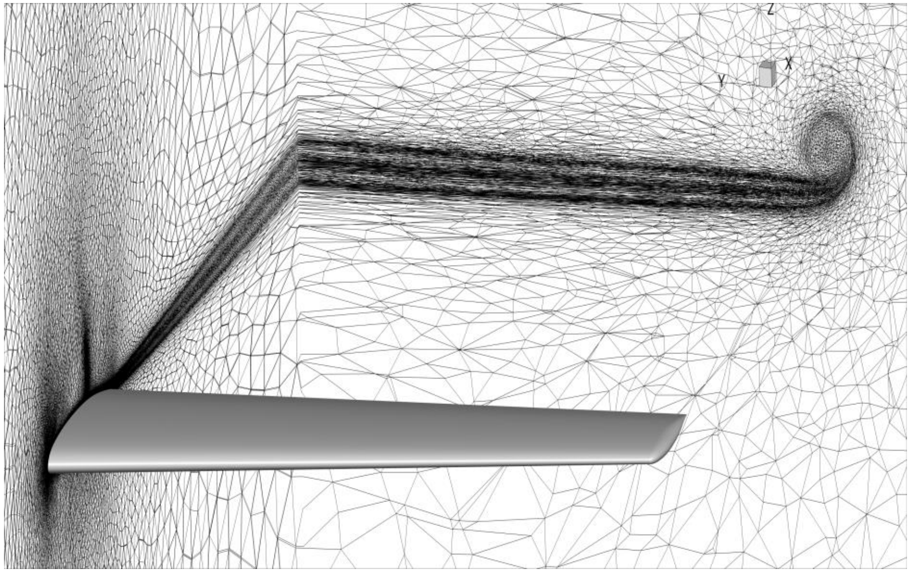

(b) pyAMG ite9 (low gradation) – ~21.3 million vertices

Both meshes: strong anisotropic clustering near wing surface, trailing edge, and wake · pyAMG mesh: more organised wake-refinement structure · Both resolve upper-surface shock, near-wall gradients, and trailing-edge vortex system

Case 2a – NASA CRM Wing/Body: Configuration & Setup (M_∞ =0.85, Re=5×10^6, α=2.5°)

Flow Conditions

- M_∞=0.85, Rec=5×10^6, α=2.5°, T=310.928 K
- Adiabatic wall, Sutherland viscosity (T_0=491.6°R)
- Far-field $\chi = \tilde{\nu}/\nu = 3$
- Deformed CRM wing/body (matches experimental test conditions)

pyAMG Adaptation Strategy

- ite0–ite9: distance-only mesh adaptation for near-wall boundary layer resolution
- ite10 onward: wall-distance + Mach sensor combined
- L^4 norm for metric computation
- Final mesh: ~75 million vertices

Reference Quantities

- S_{ref} = 191.85 m² (semi-span)
- C_{ref} = 278.5 in, b_{ref} = 1156.75 in
- Moment ref. centre: (1325.90, 0, 177.95) in

Complexity vs. Previous Cases

- Wing-body junction introduces additional flow complexity
- Transonic upper-surface shock (3D spanwise variation)
- Three-dimensional wake
- Highest geometric complexity in test cases

Case 2a – NASA CRM: Adaptive Mesh Refinement History (pyAMG)

Level (Sensor)	n_nodes	n_elements	CD	CL	CM
ite10 (Dist.+Mach)	2,143,152	12,361,337	0.03041	0.49466	-0.10730
ite11	3,576,609	20,500,021	0.02695	0.51304	-0.09874
ite15	7,184,503	41,193,365	0.02655	0.51417	-0.09945
ite18	10,981,174	63,817,141	0.02648	0.51432	-0.09969
ite19	30,253,464	176,756,636	0.02637	0.51540	-0.10048
ite20	46,961,110	276,647,509	0.02634	0.51582	-0.10052
ite21	62,477,270	369,911,377	0.02634	0.51580	-0.10049
ite22	75,024,745	445,306,114	0.02634	0.51581	-0.10049

Final converged values (ite22): CD=0.02634, CL=0.51581, CM=-0.10049

Case 2a – NASA CRM: pyAMG-Adapted Mesh Slices (ite22, 75M vertices)

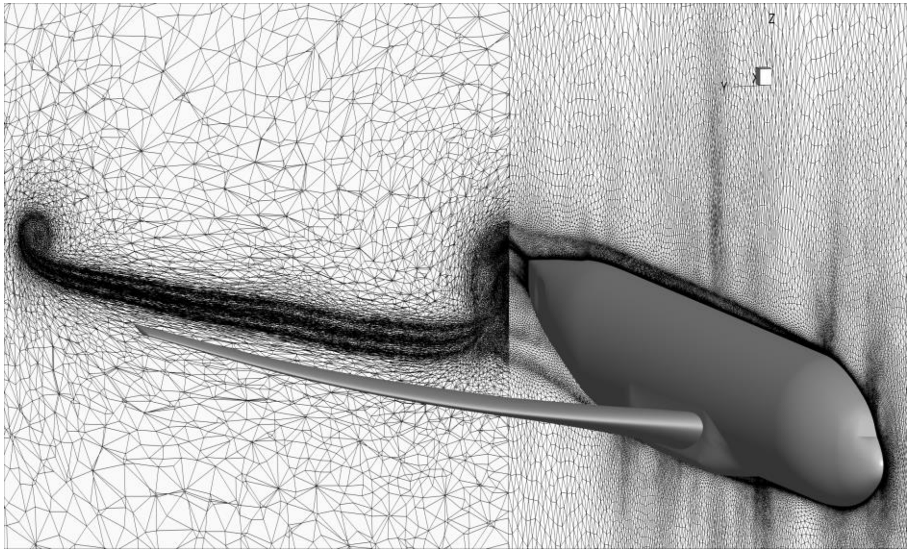

(a) Downstream wake slice + symmetry-plane

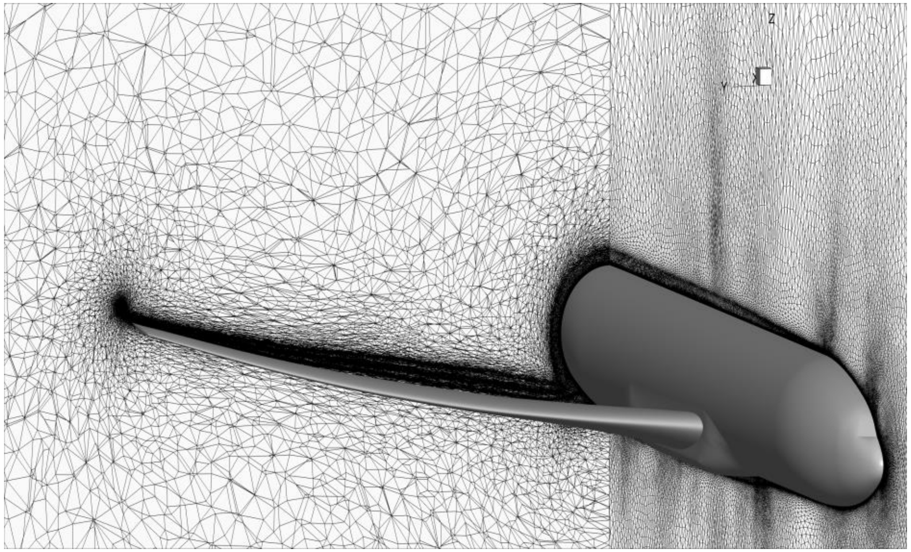

(b) Near-wing slice downstream + symmetry-plane

Strong anisotropic clustering near wing surface, trailing wake, shock-aligned region · Far field remains coarse – metric-driven selective refinement

Case 2a – NASA CRM: Spanwise Volume Mesh Slices ($\eta = y/b_{ref}$)

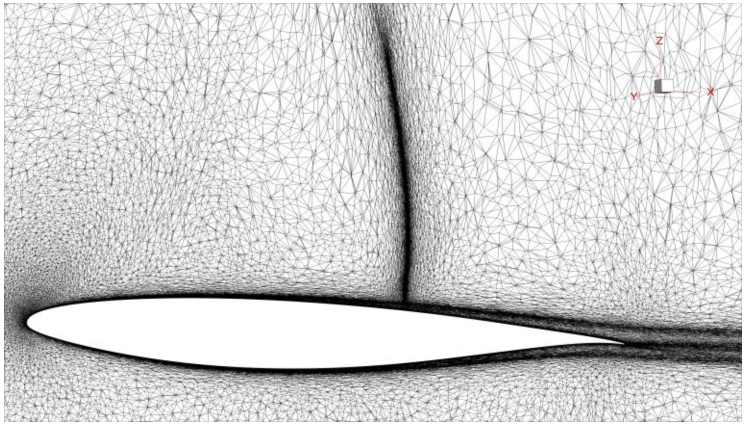

(a) η = 0.286

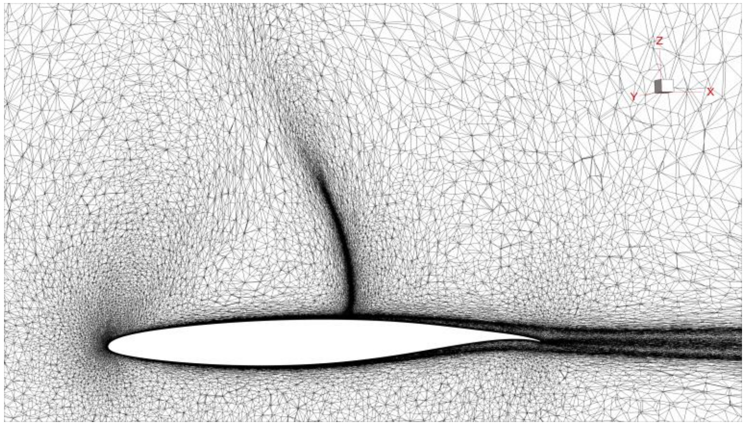

(b) η = 0.502

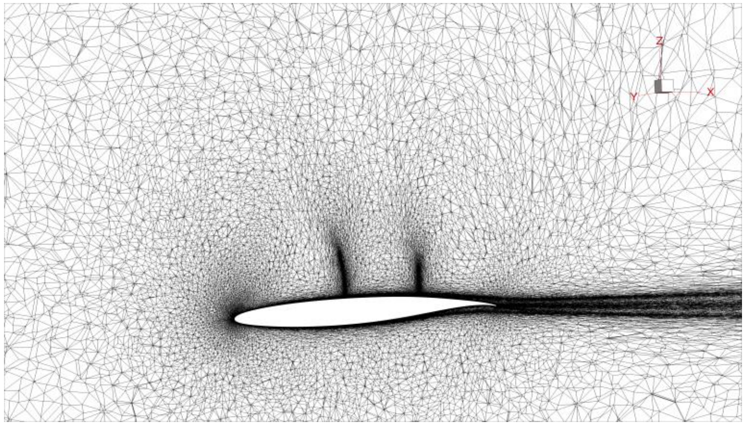

(c) η = 0.846

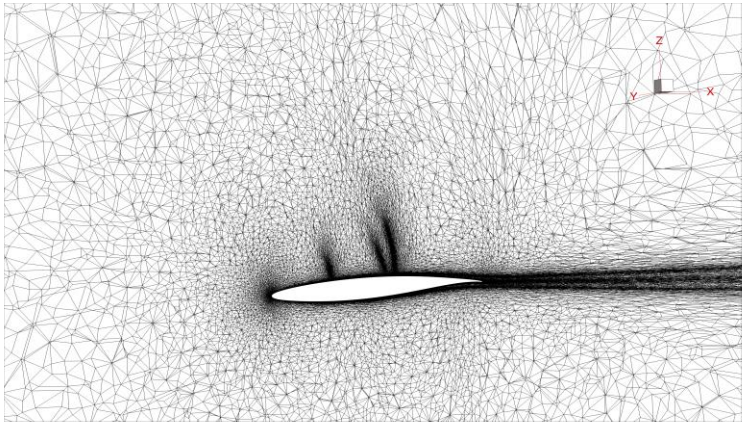

(d) η = 0.950

Near root/mid-span ($\eta \leq 0.502$): single strong shock · Near tip ($\eta \geq 0.846$): two weaker shocks

Case 2a – NASA CRM: Spanwise Mach Number Contours ($\eta = y/b_{ref}$)

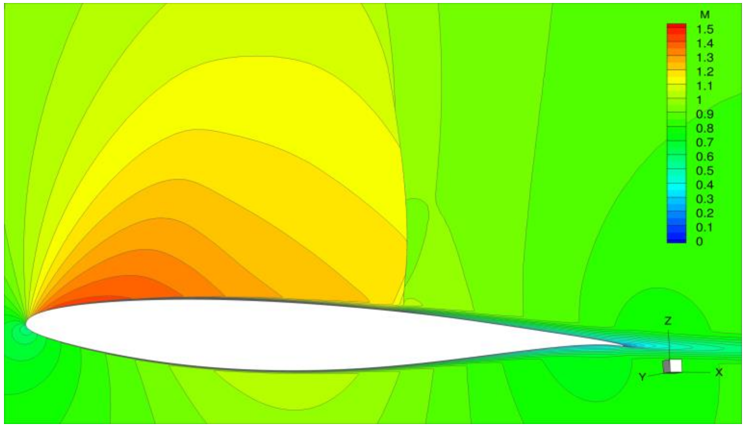

(a) η = 0.286

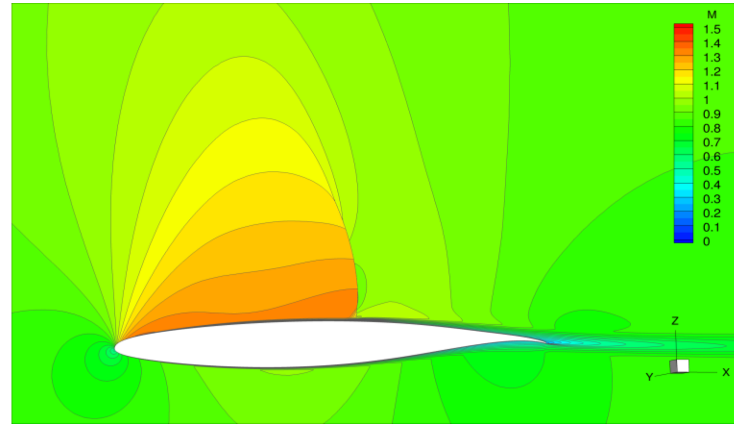

(b) η = 0.502

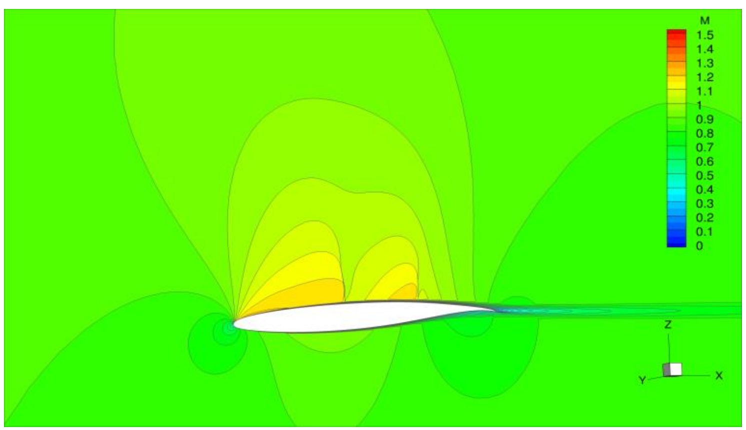

(c) η = 0.846

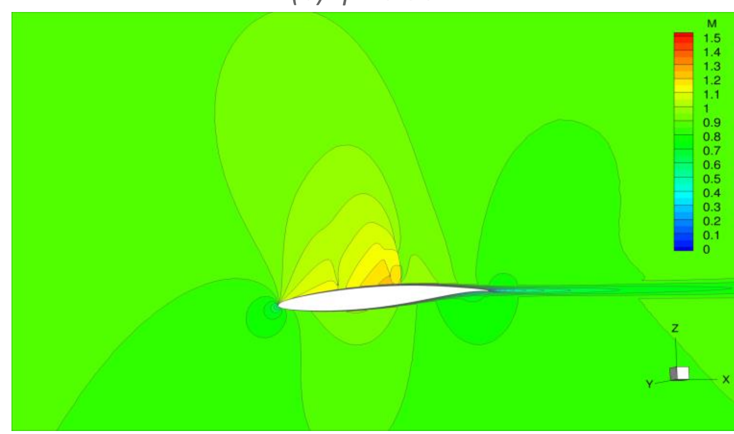

(d) η = 0.950

Near root/mid-span (η≤0.502): single strong shock · Near tip (η≥0.846): two weaker shocks

Case 2a – NASA CRM: Surface Cp Distributions at Six Spanwise Stations

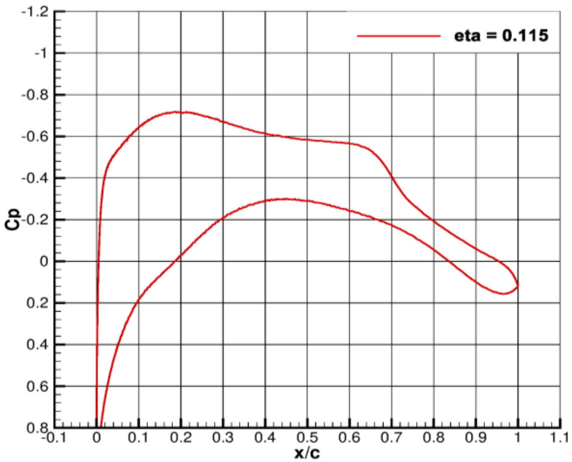

(a) η=0.115

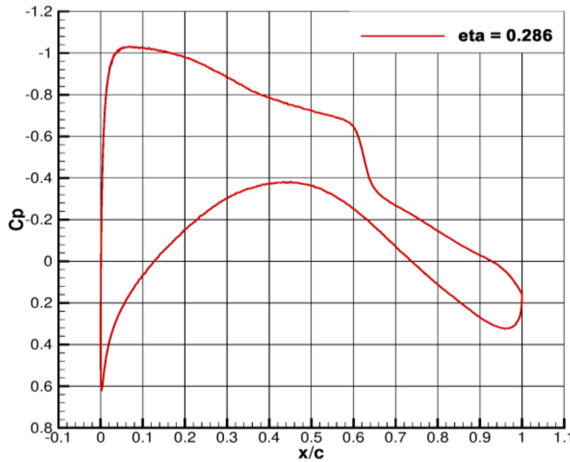

(b) η=0.286

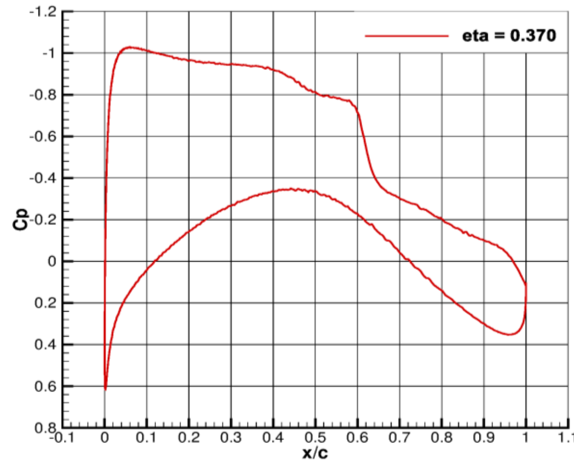

(c) η=0.370

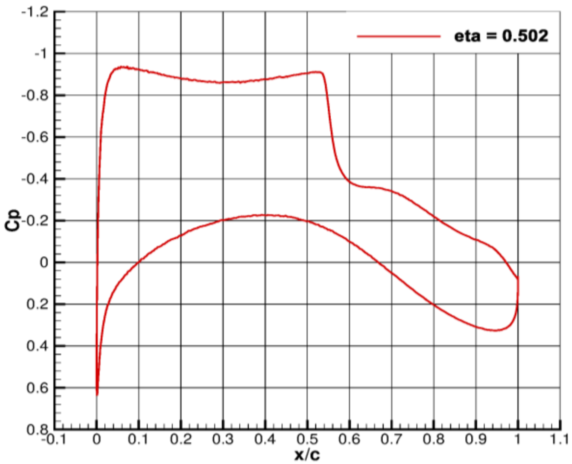

(d) η=0.502

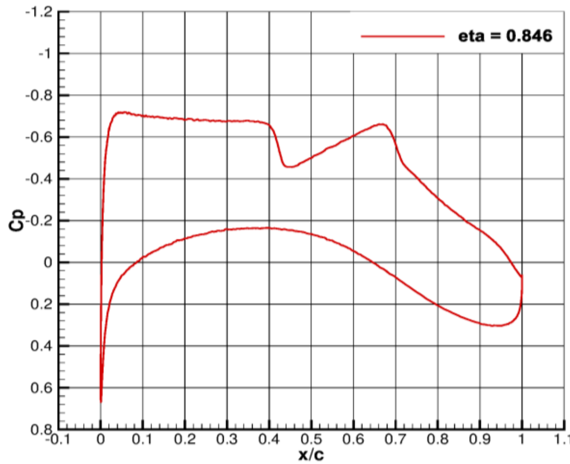

(e) η=0.846

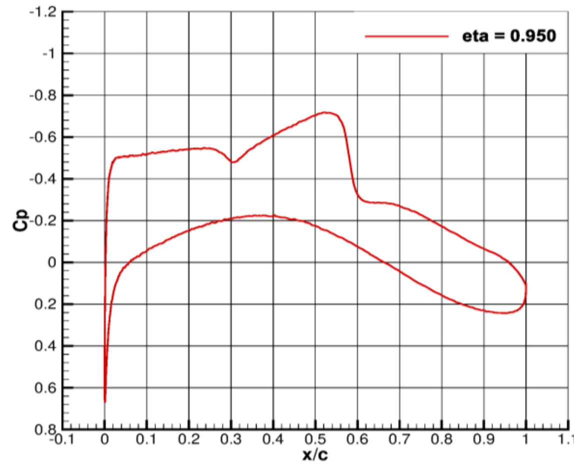

(f) η=0.950

Inboard stations (a–d): single sharp Cp jump on upper surface · Outboard stations (e–f): two distinct weaker Cp jumps near wing tip

Case 2a – NASA CRM: Residual Histories & Drag Convergence

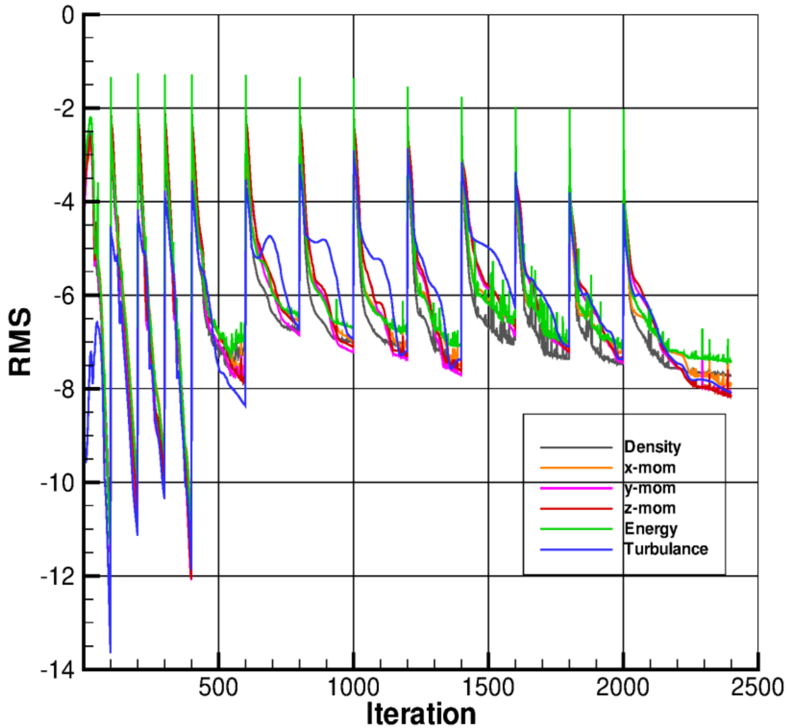

(a) Nonlinear residual histories per adaptation cycle

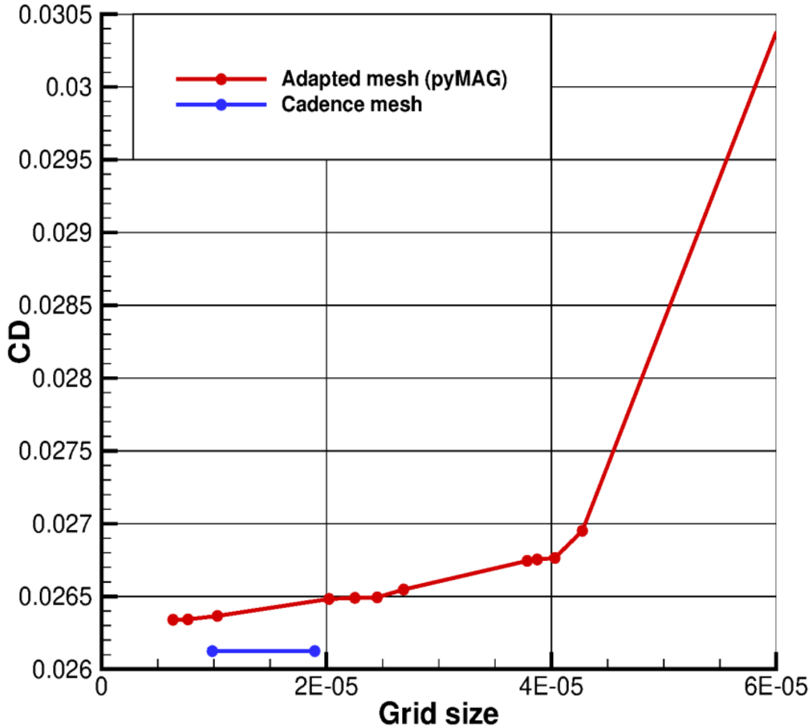

(b) CD convergence – pyAMG vs. Cadence reference

Cadence computed value: CD = 0.026124 · Final pyAMG value 2.2 drag counts above level two Cadence — offset attributed to mesh-generation strategy, not lack of convergence · Last three pyAMG levels form tight plateau

Case 2a – NASA CRM: Surface Mesh & Pressure Contours (ite22)

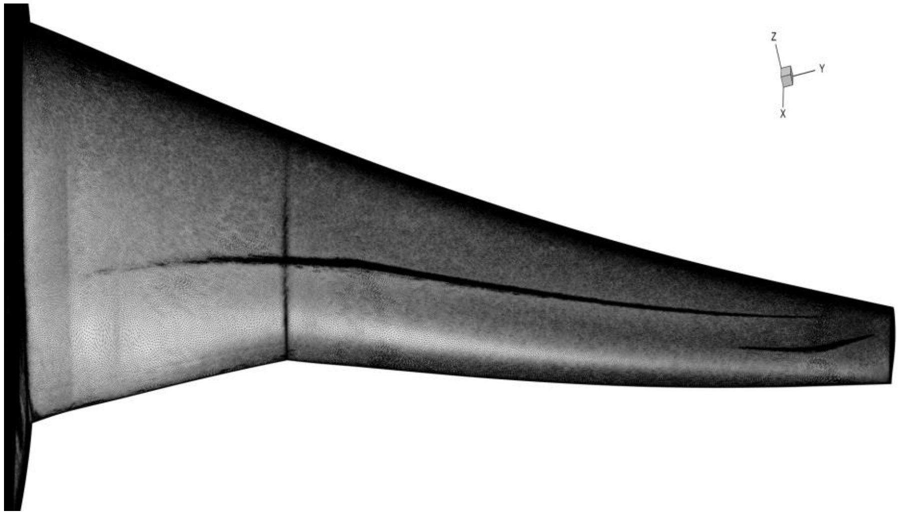

(a) pyAMG-adapted surface mesh

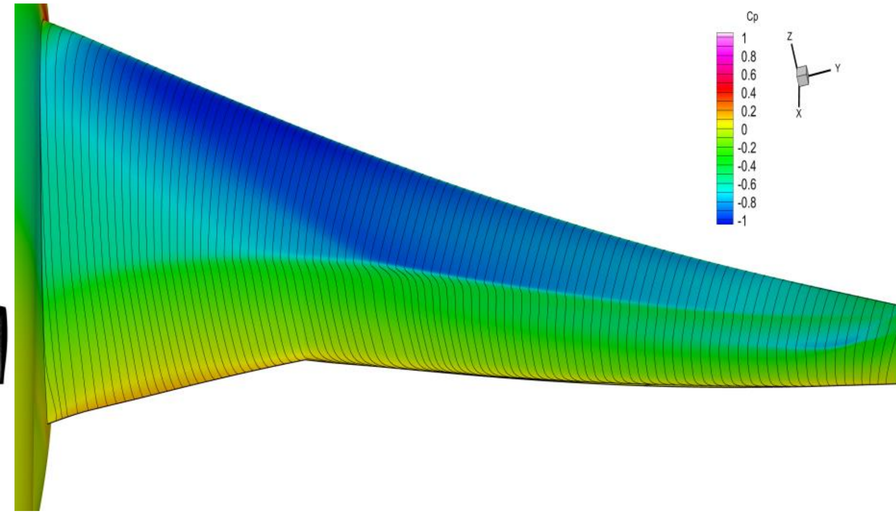

(b) Upper-surface Cp contours

Increased vertex density along shock location, wing-body junction, LE/TE · Strong upper-surface suction region terminated by clear shock line · Post-shock recovery well resolved

Conclusions

- The integration of INRIA pyAMG and NASA Refine within HEMLAB provides an efficient anisotropic mesh adaptation strategy for complex transonic configurations, reducing solution scatter and improving prediction consistency across the hierarchy of DPW-8 test cases.
- The monolithic approach based on the PETSc SNES nonlinear solver is highly robust and can achieve near machine-precision convergence for complex configurations. However, excessive refinement along shock waves can generate extremely high-aspect-ratio elements, which may hinder convergence to machine precision.
- The unweighted least-squares approach may not be sufficiently reliable near solid walls for hexahedral- and prism-based boundary-layer meshes and therefore requires special attention.
- The upwinding parameter β has a strong influence on numerical diffusion and the predicted drag coefficient. Lower values of β lead to significantly faster convergence.
- NASA Refine can be initialized from very coarse meshes using the EGADS CAD library, enabling rapid coarse-mesh convergence while providing more suitable initial conditions for the Newton solver.
- Using the Fréchet derivative leads to a more robust Newton method, which is particularly beneficial during the initial iterations. On the other hand, constructing the exact Jacobian can lead to higher CFL numbers for the final convergence.

Future Work & Limitations

Current Limitations

- Residuals do not always reach machine precision – stiffness in shock-dominated regions with strong anisotropic refinement
- Limiters (Barth–Jespersen, Venkatakrishnan–Wang, Nishikawa) implemented but NOT activated – limiter Jacobian contributions needed to improve non-linear Newton method convergence
- Unweighted least-squares gradient reconstruction may be unreliable near walls in mixed-element BL meshes (hex dominated and prism boundary layer meshes). Generally this is not an issue for pure tet meshes.
- The public versions of the NASA Refine and INRIA pyAMG libraries permit tetrahedral elements with four nodes on solid walls. This may lead to convergence issues, particularly for low-dissipation flux schemes approaching a central discretization as the Mach number tends to zero (e.g., HLLC-LM). The latest version of NASA Refine, provided by M. Park, eliminates this issue and improves convergence. However, it can create very small elements.
- pyAMG/Refine sequence based on local adaptive refinement, not systematic global refinement – convergence interpretation requires care

Future Work

- Incorporate limiter Jacobian contributions for improved Newton convergence & robustness
- Additional turbulence closures: k-ω SST, SA-QCR, for broader model sensitivity study
- Higher-order reconstruction (3rd-order) for improved accuracy
- Goal-oriented adaptation metrics for drag-specific adjoint-based error control
- Broader DPW-8 scatter comparison with other participant solvers
- Extension to unsteady configurations with ATS
- Cross diffusion effects on anisotropic high aspect ratio tet elements within boundary layer and shock should be addressed properly.

Acknowledgements

AIAA DPW Committee

Test-case definitions and reference grids

EuroHPC – etur26

Access to MareNostrum 5 supercomputer at Barcelona Supercomputing Center (BSC), Spain

TÜBİTAK ULAKBİM TRUBA and ITU National Center for High Performance Computing (UHeM)

Computational resources

Tecplot

Visualisation software licenses

Open-source libraries

PETSc, NASA refine, Inria pyAMG, EGADS/EGADSlite, TetGen, METIS, Zoltan

ITU-BAP (Project No. HIZDEP-48545)

Financial support for participation in AIAA DPW-8 and Aviation Forum 2026

Thank You!

Questions & Discussion

Ibrahim Asar
PhD Candidate, Istanbul Technical University
asar17@itu.edu.tr

Prof. Mehmet Sahin
Faculty of Aeronautics and Astronautics
Istanbul Technical University, Turkey
msahin@itu.edu.tr

References

1. Akkurt, S. and Sahin, M., "An Efficient Data Structure for Three-Dimensional Vertex-Based Finite Volume Method," *APS 70th Annual Meeting Division of Fluid Dynamics*, Denver, CO, 2017.
2. Akkurt, S. and Sahin, M., "An Efficient Edge-Based Data Structure for the Compressible Reynolds-Averaged Navier–Stokes Equations on Hybrid Unstructured Meshes," *Int. J. for Numerical Methods in Fluids*, 2022, 94:13–31.
3. Balay, S. et al., "PETSc Users Manual," ANL-95/11 – Revision 3.10, *Mathematics and Computer Science Division, Argonne National Laboratory*, 2018.
4. Barth, T. J., "A 3-D Upwind Euler Solver for Unstructured Meshes," AIAA Paper 91-1548-CP, *10th AIAA Computational Fluid Dynamics Conference*, Honolulu, HI, 1991.
5. Barth, T. J. and Jespersen, D. C., "The Design and Application of Upwind Schemes on Unstructured Meshes," AIAA Paper 89-0366, *27th Aerospace Sciences Meeting*, Reno, NV, 1989.
6. Bonet, J. and Peraire, J., "An Alternating Digital Tree (ADT) Algorithm for 3D Geometric Searching and Intersection Problems," *Int. J. for Numerical Methods in Engineering*, 1991, 31(1):1–17.
7. Devine, K. D., Boman, E. G., Riesen, L. A., Catalyurek, U. V., and Chevalier, C., "Getting Started with Zoltan: A Short Tutorial," Sandia National Laboratories Technical Report, 2009.
8. Frazza, L., "3D Anisotropic Mesh Adaptation for Reynolds-Averaged Navier–Stokes Simulations," Ph.D. Thesis, Sorbonne Université, 2018.
9. Haimes, R. and Drela, M., "On the Construction of Aircraft Conceptual Geometry for High-Fidelity Analysis and Design," AIAA Paper 2012-0683, *50th AIAA Aerospace Sciences Meeting*, Nashville, TN, 2012.
10. Haimes, R. and Dannenhoffer, J. F., "EGADSlite: A Lightweight Geometry Kernel for HPC," AIAA Paper 2018-1401, *AIAA SciTech Forum*, Kissimmee, FL, 2018.
11. Kamenetskiy, D. S., Bussoletti, J. E., Hilmes, C. L., Venkatakrishnan, V., Wigton, L. B., and Johnson, F. T., "Numerical Evidence of Multiple Solutions for the Reynolds-Averaged Navier–Stokes Equations," *AIAA Journal*, 2014, 52(8):1686–1698.
12. Karypis, G. and Kumar, V., "A Fast and High Quality Multilevel Scheme for Partitioning Irregular Graphs," *SIAM Journal on Scientific Computing*, 1999, 20(1):359–392.
13. Liou, M.-S., "A Sequel to AUSM, Part II: AUSM$^+$-up for All Speeds," *J. Comput. Phys.*, 2006, 214:137–170.
14. Loseille, A., "Metric-Orthogonal Anisotropic Mesh Generation," *Procedia Engineering*, 2014, 82:403–415.
15. Loseille, A. and Alauzet, F., "Continuous Mesh Framework Part I & Part II," *SIAM Journal on Numerical Analysis*, 2011, 49(1):38–86.
16. Mavriplis, D. J., Vassberg, J. C., Tinoco, E. N., et al., "Grid Quality and Resolution Issues from the Drag Prediction Workshop Series," AIAA Paper 2008-0930, *46th AIAA Aerospace Sciences Meeting*, Reno, NV, 2008.

17. Nishikawa, H., "New Unstructured-Grid Limiter Functions," AIAA Paper 2022-1374, *AIAA SciTech 2022 Forum*, San Diego, CA, 2022.
18. Okan, A., "Fully-Coupled k–ω SST Turbulence Model Implementation for Nonlinear Newton Method in HEMLAB," M.Sc. Thesis, Istanbul Technical University, 2025.
19. Park, M. A., Balan, A., Anderson, W. K., et al., "Verification of Unstructured Grid Adaptation Components," AIAA Paper 2019-1723, *AIAA SciTech Forum*, San Diego, CA, 2019.
20. Roe, P. L., "Approximate Riemann Solvers, Parameter Vectors, and Difference Schemes," *J. Comput. Phys.*, 1981, 43(2):357–372.
21. Si, H., *TetGen: A Quality Tetrahedral Mesh Generator and 3D Delaunay Triangulator, User's Manual, Version 1.6*, Weierstrass Institute, 2020.
22. Spalart, P. R. and Allmaras, S. R., "A One-Equation Turbulence Model for Aerodynamic Flows," *La Recherche Aérospatiale*, 1994, 1:5–21.
23. Allmaras, S. R., Johnson, F. T., and Spalart, P. R., "Modifications and Clarifications for the Implementation of the Spalart–Allmaras Turbulence Model," ICCFD7-1902, *7th Int. Conf. on Computational Fluid Dynamics*, Big Island, HI, 2012.
24. Sukas, H. and Sahin, M., "HEMLAB Algorithm Applied to the High-Lift JAXA Standard Model," AIAA Paper 2021-1994, *AIAA SciTech 2021 Forum*, Virtual Event, 2021.
25. Sukas, H. and Sahin, M., "HEMLAB Algorithm Applied to the 4th AIAA CFD High Lift Prediction Workshop," AIAA Paper 2022-3809, *AIAA AVIATION 2022 Forum*, Chicago, IL, 2022.
26. Sukas, H. and Sahin, M., "HEMLAB Algorithm Applied to the High-Lift Japan Aerospace Exploration Agency Standard Model," *Journal of Aircraft*, 2024. DOI: 10.2514/1.C037849
27. Sukas, H. and Sahin, M., "A Robust Monolithic Nonlinear Newton Method for the Compressible Reynolds-Averaged Navier–Stokes Equations," *Computers & Fluids*, Vol. 289, 2025, Article 106549. DOI: 10.1016/j.compfluid.2025.106549
28. Sukas, H., "Metric-Based Mesh Adaptation Methodology Applied to HEMLAB Algorithm," Ph.D. Thesis, Istanbul Technical University, Advisor: Prof. Dr. Mehmet Şahin, June 2025.
29. Toro, E. F., Spruce, M., and Speares, W., "Restoration of the Contact Surface in the HLL Riemann Solver," *Shock Waves*, 1994, 4:25–34.
30. Vassberg, J. C., Tinoco, E. N., Mani, M., et al., "Summary of the Third AIAA CFD Drag Prediction Workshop," AIAA Paper 2007-0260, *45th AIAA Aerospace Sciences Meeting*, Reno, NV, 2007.
31. Vassberg, J. C., DeHaan, M. A., Rivers, M., and Wahls, R. A., "Development of a Common Research Model for Applied CFD Validation Studies," AIAA Paper 2008-6919, *26th AIAA Applied Aerodynamics Conference*, Honolulu, HI, 2008.
32. Venkatakrishnan, V., "Convergence to Steady State Solutions of the Euler Equations on Unstructured Grids with Limiters," *Journal of Computational Physics*, 1995, 118(1):120–130.
33. Wyman, N. J., Park, M. A., Baker, P., and Chawner, J. R., "A Framework for Mesh–Geometry Associativity During Mesh Adaptation," AIAA Paper 2021-1900, *AIAA SciTech 2021 Forum*, Virtual Event, 2021.
34. Akgün, H., Asar, I., and Sahin, M., "HEMLAB Algorithm Applied to HIOCFD Delta Wing and OTC1 Missile," AIAA Paper 2023-4403, *AIAA AVIATION 2023 Forum*, San Diego, CA, 2023.
35. Drag Prediction Workshop Committee, *DPW-8 Scatter Results – Test Case 1b: Joukowski Mesh*, GitHub, 2023. https://github.com/Drag-Prediction-Workshop/DPW8-Scatter